Article

J. Mex. Chem. Soc. **2021**, *65*(4)
Regular Issue

ISSN-e 2594-0317

A Novel Efficient MPEG-Chitosan/HA Biopolymer for Adsorption of the Anticancer SN-38 Liquid Dispersions: Kinetics, Thermodynamic and *Ex-Vivo* Release Evaluation

Faezeh Sharifi[1], Mansour Jahangiri[1*], Pedram Ebrahimnejad [2,3*]

[1]Faculty of Chemical, Petroleum and Gas Eng., Semnan University, Semnan, Zip code: 35196-45399, I.R. Iran.
[2]Department of Pharmaceutics, Faculty of Pharmacy, Mazandaran University of Medical Sciences, Sari, I.R. Iran.
[3]Pharmaceutical Sciences Research Center, Hemoglobinopathy Institute, Mazandaran University of Medical Sciences, Sari, I.R. Iran.

***Corresponding author:** Mansour Jahangiri, email: mjahangiri@semnan.ac.ir; Pedram Ebrahimnejad, e-mail: pebrahimnejad@mazums.ac.ir

Received January 25th, 2021; Accepted June 15th , 2021.

DOI: http://dx.doi.org/10.29356/jmcs.v65i4.1505

Abstract. Amongst several drug delivery schemes for perfect drug delivery comprise biocompatibility, selective aiming of cancer cells, low-cost, and safe process of nanoparticle preparation. In this work, a new mPEG-chitosan/HA biopolymer was prepared as adsorbent nanoparticles (mNPs) for an efficient drug delivery system. The mNPs was synthesized by conjugating poly (ethylene glycol) methyl ether (mPEG) to chitosan and prepared through ionic gelation between mPEG-chitosan and hyaluronic acid (HA). The prepared mNPs were used to adsorption/release of 7-ethyl-10-hydroxycamtothecin (SN-38) from its liquid dispersions. The mNPs adsorbent was characterized by Fourier transforms infrared spectroscopy (FT-IR), differential scanning calorimetry (DSC), scanning electron microscopy (SEM). The results demonstrated that the adsorption isotherm of SN-38 on mNPs follows Langmuir model, and the adsorption capacity was 346.511 mg g^{-1}. Besides, the pseudo-first order kinetic well fitted the equilibrium data. Further, thermodynamic parameters including ΔH, ΔG and ΔS were calculated which demonstrated that the physical spontaneous adsorption was prevailing. In addition, the *ex- vivo* release of SN-38 from mNPs were in good agreement with Korsmeyer-Peppas equation indicating the drug release process was governed by diffusion phenomena. The above results revealed that mNPs containing SN-38 was a good candidate for the drug delivery systems.
Keywords: Nanoparticles; adsorption; kinetics; thermodynamics; *ex-vivo* release.

Resumen. Dentro de las diferentes propiedades importantes de los sistemas de liberación de fármacos se encuentran la biocompatibilidad, el ataque selectivo a las células cancerosas, el bajo costo y los procesos adecuados de preparación de nanopartículas. En este trabajo, un nuevo biopolímero de mPEG-chitosan/HA se preparó en la forma de nanopartículas (mNPs) para el uso como un sistema de liberación controlada de fármacos. Las nanopartículas se sintetizaron incorporando el éter metílico de poli(etilenglidol) al quitosano, y se prepararon a través de la gelación iónica entre el mPEG-quitosano y el ácido hialurónico (HA). Las nanopartículas así preparadas se probaron en su efectividad para la absorción y liberación de 7-etil-10-hidroxicamtotecina (SN-38) en forma de dispersiones líquidas. El absorbente hecho a partir de las nanopartículas se caracterizó mediante espectroscopía infrarroja de transformada de Fourier (FT-IR), calorimetría diferencial de barrido (DSC) y microscopía electrónica de barrido (SEM). Se encontró que la isoterma de adsorción de la muestra de nanopartículas conteniendo SN-38 se ajusta al modelo de Langmuir, siendo el valor de la capacidad de adsorción de 346.511 mg g^{-1}. El modelo cinético de seudo primer orden se

J. Mex. Chem. Soc. **2021**, *65*(4)
Regular Issue

ISSN-e 2594-0317

ajusta adecuadamente a los datos obtenidos al equilibrio. Más aún, los parámetros termodinámicos tales como ΔH, ΔG and ΔS se pudieron calcular, lo que indica que la adsorción física espontánea es el mecanismo que prevalece. Además, los datos de liberación *ex- vivo* de SN-38 a partir de las nanopartículas se pueden ajustar a la ecuación de Korsmeyer-Peppas, indicando que el proceso de liberación del fármaco está gobernado por un proceso de difusión. Los resultados anteriores indican que el sistema de nanopartículas conteniendo SN-38 es un buen candidato para desarrollar un sistema de liberación controlada de fármacos.
Palabras clave: Nanopartículas; adsorción; cinética; termodinámica; liberación *ex-vivo*.

Introduction

Over the 21st century, 7-ethyl-10-hydroxycamtothecin (SN-38) is considered a major potent anticancer agent because of its promising anticancer activity for different types of human cancer [1, 2]. Nonetheless, some major drawbacks limited the clinical application of SN-38 including poor water solubility, low stability in physiological pH, conversion to carboxylate form, and gastrointestinal toxicity [3]. As a consequence, innovative new carriers should be employed as a drug delivery system for SN-38 to improve SN-38 pharmacokinetics. At present, many conventional drug carriers have been developed for delivery of SN-38 including inorganic nanoparticles [4, 5] polymeric nanoparticles [6] dendrimers [7] and micelles [8]. The most significant criteria that must be employed for an ideal drug delivery system include biocompatibility, high drug loading, minimum side effects, selective targeting of cancer cells, low-cost, and safe method of nanoparticle preparation with low amounts of organic and toxic solvents [9].

Among various drug delivery systems, biodegradable polymeric nanoparticles are well- known thanks to their attractive features such as fewer side effects, sustained release, and low dosage [10]. HA is a natural biodegradable polymer and extracellular constituent including D-Glucuronic acid and N-acetyl-D-Glucosamine units. In different types of cancer, the interaction between HA and specific cellular receptors such as CD44 is used as a targeting moiety for many cancerous tissues [11,12]. Another biodegradable polymer, chitosan, has received a great deal of attention due to non-toxic properties, biodegradability, and biocompatibility. It consists of N-acetyl-d-glucosamine and D-glucosamine units [13]. For the existence of amine groups on the structure of chitosan, chitosan is positive in acidic and neutral pHs, and able to form intermolecular complexes with polyanions such as HA [14]. Poly (ethylene glycol) methyl ether (mPEG) is an amphiphilic polymer that acts as a hydrophilic shell to protect nanoparticles from plasma proteins and reduce clearance by the mononuclear phagocyte system while also increasing the circulation time in the body [15]. The hydrophilic nature of the mPEG causes greater physical or chemical drug adsorption onto the surface of nanoparticles and reduces the drug denaturation. Meanwhile, adding the mPEG to the other biopolymer (PEGylation) increases the bioavailability of the delivery system while increasing the loading capacity [16]. Among various chemotherapy treatments, oral chemotherapy has opened a new opportunity towards "therapy at home". Oral chemotherapy can improve the quality of life of patients with advanced and metastatic cancer. [17]. Polyelectrolyte complexation between HA and mPG-chitosan causes the formation of mNPs with potential for oral delivery.

The drug and the drug delivery system interaction offer valuable information about the drug dosage and its release mechanism. Physical or chemical loading are two significant criteria that influence the toxicity and side effects. Physical adsorption is favorable because of dispensing with the use of chemical reactions and toxic junction reagents [18].

Previously, the literature revealed that most physical adsorption of SN-38 onto drug delivery systems was performed by employing nanotubes [3,19,20]. Indeed, carbon nanotubes proved a good candidate for drug delivery systems, but the consumption of massive energy in the process and purification to prevent unwanted carbon reactions are some limitations of carbon nanotube usage in drug delivery systems [21]. According to the literature, supramolecular nanoparticles and poly amino acid micelle was used as nanocarriers to adsorb camptothecin (SN-38), but the adsorption capacity was low as the drug aggregated during the adsorption [22,23]. Zhuang et al. reported zeolitic imid-azolate framework-8 (ZIF-8) nanospheres as adsorbent of camptothecin. The results showed that a smaller particle size can facilitate cellular uptake, but the drug adsorption capacity was lower than 10 mg g-1 [24]. Chi *et al*. used biocompatible methoxy poly (ethylene

J. Mex. Chem. Soc. **2021**, *65*(4)
Regular Issue

ISSN-e 2594-0317

glycol)-b-poly(ε-caprolactone) (mPEG–PCL) nanoparticles to adsorb camptothecin where the maximum adsorption capacity was 96 mg g^{-1} [25]. Many studies to overcome of SN-38 solubility and enhancing bioavailability have proposed using various drug delivery systems, including expensive polymers. They also suffer time-consuming preparation methods and the use of toxic or organic solvents. Most of these drug delivery systems are not environmentally friendly or cause toxic or side effects [26]. In this study, the physical adsorption of SN-38 drug on mNPs was investigated. The adsorption isotherm, kinetics and thermodynamics of SN-38 on mNPs have studied. Thus, in this work, we attempted to design a novel nanocarrier using chitosan, mPEG and HA as main ingredients (mNPs) to improve the stability and delivery of SN-38 in physiological media (pH 7.4) as well as increasing the sustained release of this drug. To achieve the optimum delivery for SN-38, initially mPEG-chitosan was synthesized and then was developed through ionic gelation between mPEG-chitosan and hyaluronic acid (HA) for CD44 receptor. Then, the adsorption of SN-38 in liquid dispersion on mNPs was investigated via adsorption isotherm, kinetics and thermodynamics. The mNPs were characterized by FT-IR, DSC, and SEM. Furthermore, the pharmacokinetics of sustained release of SN-38 anticancer was investigated from rat intestines under *ex-vivo* conditions.

Experimental

Materials And Methods

Chemicals

Low molecular weight chitosan (50 kDa) with the deacetylation degree of 75-85 % was purchased from Sigma Aldrich (St. Louis, MO USA). Hyaluronic acid sodium salt (HA) was obtained from Solarbio® (Beijing, China). Poly (ethylene glycol) methyl ether (mPEG) with the molecular weight 5000, sodium hydroxide (NaOH), glacial acetic acid, hydrochloric acid (HCl), and dimethylsulfoxide (DMSO) were obtained from Sigma Aldrich (Männedorf, Switzerland). SN-38 was obtained from ABRTA CO. (Shaanxi, China). Deionized water was used in all experiments. All other chemicals and reagents used were of analytical grade and obtained from commercial sources.

Methods

Synthesis of mPEG-chitosan conjugate

The chitosan was PEGylated through amide bond formation between mPEG and chitosan. In the synthesis process, 1 g of chitosan was dissolved in 10 mL of formic acid as a solvent, whereby a viscose solution was formed. Afterwards, 1 g of mPEG was added to the mixture and agitated for 15 min. Then, 1 ml of formaldehyde was added dropwise into the solution under constant stirring for 60 min. The NaOH (2 M) solution was added to the mixture to neutralize it. The obtained solution was dialyzed (MWCO: 12000-14000, Sigma-Aldrich, Germany) against deionized water for 24 h with exchanging water sequentially after which the product was lyophilized (alpha 1-2 ld plus, Martin Christ GmbH, Germany) and stored in a fridge for further use [27].

Preparation of mNPs

mNPs were prepared according to the ionic gelation method as described previously by Yang et al. with minor modifications [28]. Specifically, 0.5 mg of mPEG-chitosan was dissolved in 5 mL of deionized water containing 1 % (w/v) acetic acid for 30 min and the pH was adjusted at 3.78 utilizing 1 M NaOH. HA at a concentration of 0.5 mg ml^{-1} was dissolved in 5 mL deionized water, after which two solutions were mixed and stirred for 3 h. Thereafter, SN3-8 at a concentration of 10 % (w/v) of the polymeric solution was dissolved in DMSO for 1 h. The SN-38 solution was added to the reaction mixture dropwise under constant magnetic stirring at 800 rpm for 6 h at 25 °C.

Afterward, the solution was sonicated by a probe sonicator (bandelin electronic type GM 3100, Berlin, Germany) for 2 cycles (60 seconds on – 60seconds off) with power 400 w. The prepared mNPs were dialyzed (MWCO: 12000-14000, Sigma-Aldrich, Schnelldorf, Germany) in deionized water for 24 h and then the obtained mNPs were freeze-dried.

J. Mex. Chem. Soc. **2021**, *65*(4)
Regular Issue

ISSN-e 2594-0317

Characterization of mNPs

Particle size distribution and surface charge

Differential laser scattering method (DLS Zetasizer Nano ZPS instrument, Malvern, Worcestershire, UK) was used to evaluate the mean size, PDI, and zeta potential of the obtained mNPs. Specifically, 2 mg of samples was diluted to 4 mL with deionized water. Each measurement was carried out in triplicate.

Morphology of mNPs

Scanning electron microscopy (SEM) (SEM, Oxford Instruments, Abingdon, UK) was used to observe the morphology of mNPs. The lyophilized mNPs were fixed on an aluminum disk at room temperature, coated with gold by a sputter coater, and evaluated at 15 kV using 6300 fields.

Fourier transforms infrared (FT-IR) analysis

The FT-IR spectra of all samples were analyzed by a spectrometer (Agilent Cary 630 FTIR spectrometer, Waldbronn, Germany). The spectrum was recorded from 400-4000 cm^{-1} at a resolution of 4 cm^{-1}.

Differential scanning calorimetry (DSC)

Differential scanning calorimetry (DSC-823, Mettler Toledo, Geneva, Switzerland) was used to investigate the thermal properties of NPs. Samples were sealed in aluminum pans and heated from 30 to 300 °C with a heating ramp 10 °C min^{-1} under a nitrogen atmosphere at the flow rate of 50 cm^3 min^{-1}.

Adsorption isotherm

Different amounts of SN-38 (1.5-15 mg) were dissolved in DMSO solution and mixed with 11 mg of which is dissolved in water under constant magnetic stirring at 800 rpm for 6 h at 25 °C, thus SN-38 adsorbed on the surface of mNp. Afterwards, the solutions were centrifuged at 10,000 rpm for 20 min at 4 °C. The suspension was filtered with the final concentration of supernatants determining the absorbance of the samples at a wavelength of 265 nm by UV-vis spectrophotometer (UV-2450, Shimadzu, Japan). The adsorbed amount of SN-38 on mNPs was determined according to Equation (1):

$$q_e = (\frac{C_0 - C_e}{m})V \quad (1)$$

Where, q_e represents the adsorption capacity at time intervals (mg g^{-1}), C_0 and C_e denote the concentration of SN-38 before and after adsorption (mg L^{-1}), V is the sample volume (L), and m denotes the adsorbent mass (g) [29].

Adsorption kinetics

Adsorption kinetic experiments were performed at various concentrations of SN-38 (1.5-15 mg ml-1) with 11 mg of mNPs in 22 mL of water in a pH of 3.7 and ionic strength of 0.65 M. At predetermined intervals, the samples were withdrawn and centrifuged at 10,000 rpm for 20 min. The suspension was filtered with the final concentration of supernatants determining the absorbance of the samples at a wavelength of 265 nm using a UV-vis spectrophotometer (UV-2450, Shimadzu, Japan). The amount of SN-38 adsorbed on mNPs was calculated by Equation (2):

$$q_t = (\frac{C_0 - C_e}{m})V \quad (2)$$

Where, q_t represents the adsorption capacity at time intervals (mg g-1), C0 and Ct denote the concentration of SN-38 before and after adsorption (mg L-1), V is the sample volume (L), and m denotes the adsorbent mass (g)[29].

J. Mex. Chem. Soc. **2021**, *65*(4)
Regular Issue

ISSN-e 2594-0317

Adsorption Thermodynamics

In order to evaluate the thermodynamic properties of SN-38 adsorption on mNPs, initial concentrations of SN-38 ranging from 1.5-15 mg were added into 22 mL solution containing 11 mg of mNPs. The samples were mixed to reach equilibrium at 298, 303, 308, 313, 318, and 323 K respectively [29].

Release of SN-38 from mNPs

In order to examine the release of SN-38 adsorbed on mNPs, 25 mg of mNPs containing SN-38 was dispersed in 5 mL phosphate buffer saline (PBS). Also, 10 cm of the large intestine of a male rat was removed and washed three times with Krebs-Ringer bicarbonate solution, pH 7.4. One side of the intestine was tied and the mNPs suspension was poured into the intestine by a needle with the intestine placed in a tube with 50 mL of phosphate buffer saline (PBS). At predetermined intervals, 1 mL of the PBS was collected, and 1 mL of fresh PBS was added to the medium to keep sinking conditions. The collected PBS was mixed with 1 mL of DMSO to extract SN-38 with the amount of SN-38 measured by HPLC. The HPLC method was used to show the extent of drug release in the solution as a percentage of the drug released to the drug accumulated (the drug already released in the medium at pH of 7.4) [30].

Results and discussion

Synthesis and characterization

The obtained mNPs were measured by DLS. As shown in Fig. 1**(A)**, the size of the mNPs was 226 nm and the surface morphology was evaluated by SEM. As presented in Fig. 1**(B)**, a homogenous surface, with smaller and uniform mNPs and narrow size distribution has formed. No aggregation and clumping were observed.

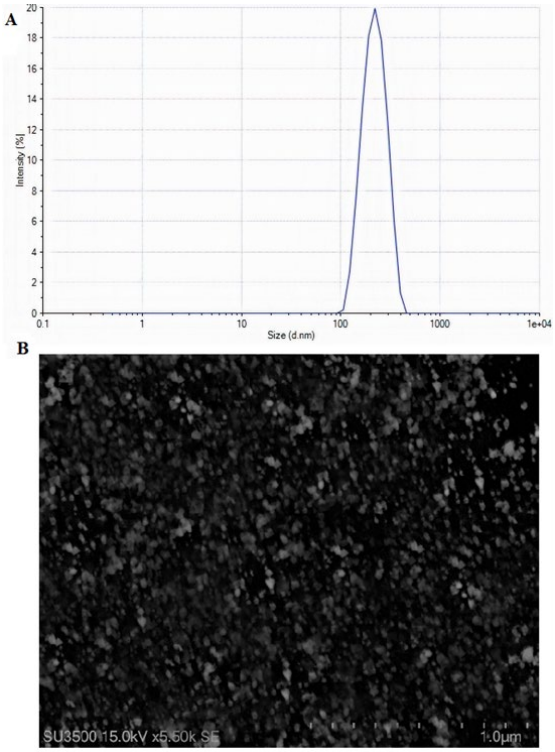

Fig. 1. (A) Particle size and distribution (DLS) and **(B)** SEM image of prepared mNPs.

J. Mex. Chem. Soc. **2021**, *65*(4)
Regular Issue

ISSN-e 2594-0317

Fourier transforms infrared spectroscopy (FT-IR)

IR spectra were studied to characterize the interaction between polymers and SN-38. Fig. 2**(A)** displays the bands within 3292.847-3363.701 cm^{-1} (N-H and O-H are stretching), as well as at 2869.057 and 2923.660 cm^{-1} (C-H symmetric and asymmetric stretching), at 1590.020 cm^{-1} (N-H is bending of the primary amine), at 1153.310 cm^{-1} (asymmetric stretching of the C-O-C bridge), at 1066.539 and 1022.056 cm^{-1} (C-O is stretching), at 1260.455 cm^{-1} bending vibrations of hydroxyls in chitosan. Fig. 2**(B)** reveals the peaks of mPEG at 2881.703 cm-1 and 1466.226 cm^{-1} (C-H stretching and C-H scissoring), at 2881.703 cm^{-1} (O-H stretching), and at 1098.614 cm^{-1} and 1279.265 cm^{-1} (C-O stretching). In Fig. 2**(C)**, mPEG-chitosan showed a peak at1582.259 cm^{-1} (a crosslinking bond due to the reaction between chitosan and mPEG). There was a disappearance of the broad peak of mPEG in mPEG-chitosan, indicating that the free hydroxyl group of mPEG reacted with the amine group of chitosan. In Fig. 2**(D)**, the peaks at 1607.538 cm^{-1} and 1720.377 cm^{-1} are associated with amide and carbonyl bonds of glucuronic and *N*-acetyl–glucosamine of HA, respectively and the peak at 1032.678 cm^{-1} is attributed to C-OH linkage stretching.

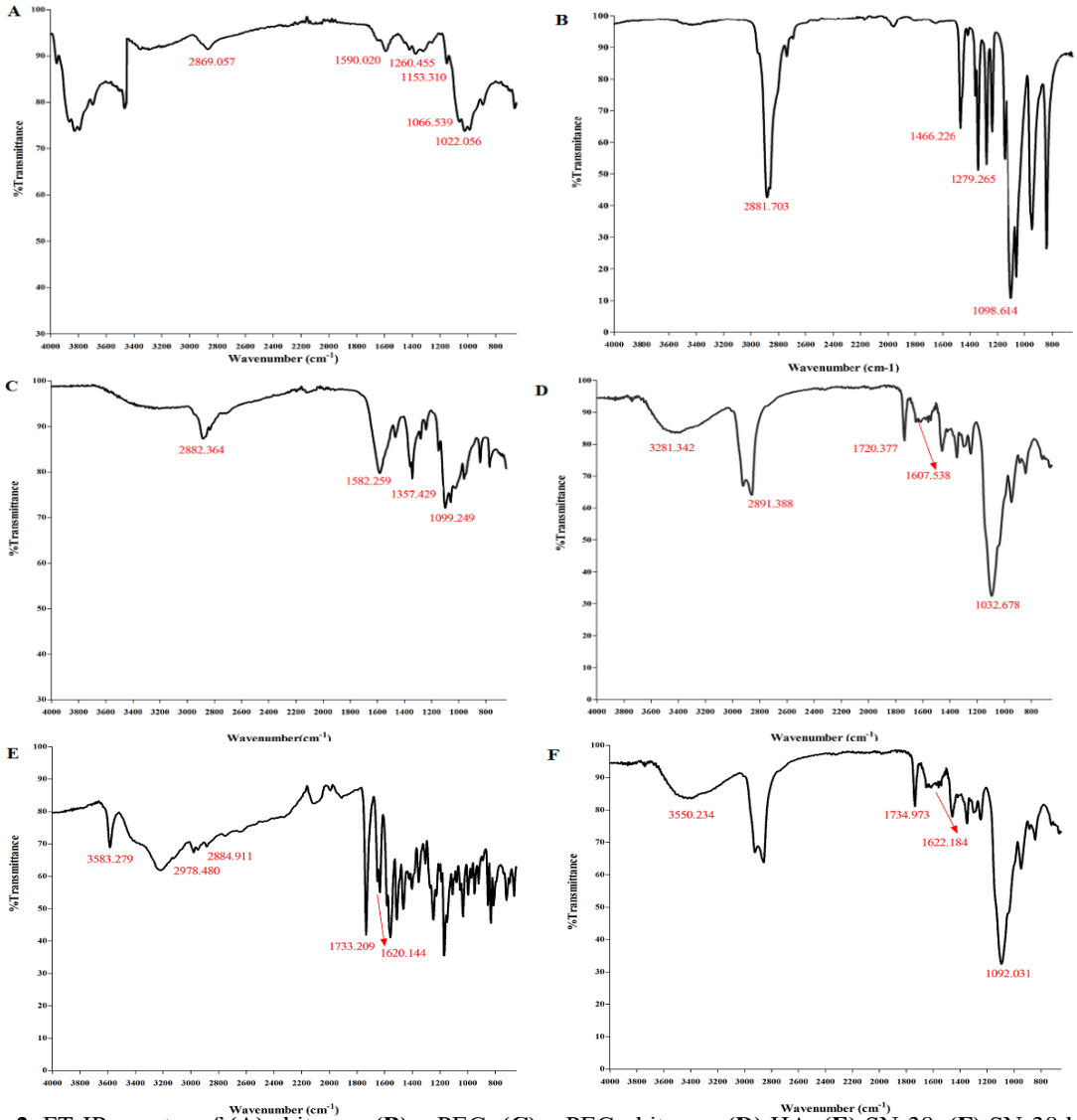

Fig. 2. FT-IR spectra of **(A)** chitosan, **(B)** mPEG, **(C)** mPEG-chitosan, **(D)** HA, **(E)** SN-38, **(F)** SN-38 loaded mNPs.

J. Mex. Chem. Soc. **2021**, *65*(4)
Regular Issue

ISSN-e 2594-0317

Differential scanning calorimetry (DSC)

The differential scanning calorimetry was conducted to investigate the thermal properties and the physical state of the drug in mNPs. The amorphous or crystalline properties of the drug can affect the in vitro and in vivo release. Chitosan exhibited an endothermic peak at 140 °C in Fig. 3, and HA showed a broad peak at 106 °C along with an exothermic peak at 239 °C. SN-38 showed an endothermic melting point at 287 °C and a characteristic peak at 225 °C, both peaks have disappeared in the thermogram of mNPs Fig. **3(D)**, this result could be that the SN-38 transformed into an amorphous state in mNPs. The amorphous state of SN-38 had better wettability and exhibited significant pharmacokinetic properties [31]. Finally, the disappearance of HA peaks indicated the interaction between HA, chitosan, and SN-38.

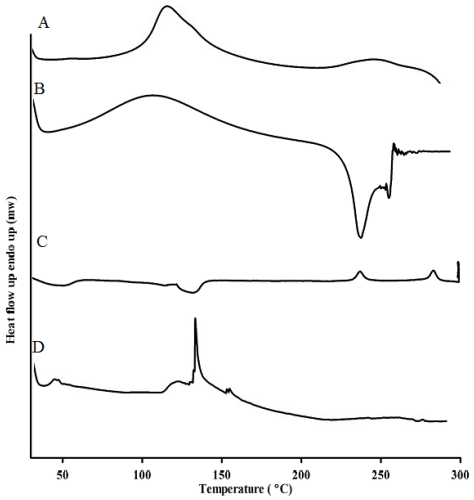

Fig. 3. DSC thermogram of: **(A)** chitosan, **(B)** HA, **(C)** SN-38, **(D)** SN-38 loaded mNPs.

Adsorption isotherm study

Adsorption isotherm models including Langmuir, Freundlich, Temkin, and Sips were used to analyze the equilibrium isotherm data. The match between the models and equilibrium data was evaluated based on the determination coefficient (R^2).

Fig. 2**(E)** demonstrates two peaks at 1733.209 cm^{-1} (lactone ring) and at 1620.144 cm^{-1} (carbonyl amide group of pure SN-38). In the spectra of SN-38 a peak occurred at 3583.279 cm^{-1} (hydrogen bonded OH) and peaks at 2978.480 and 2884.911 cm^{-1} (C-H stretching alkanes) were observed. In Fig. 2**(F)**, the peaks at 1734.973 cm^{-1} and 1622.184 cm^{-1} (the lactone ring and carbonyl group) confirm the adsorption of SN-38 on the surface mNPs and the lactone form of SN-38 is protected which is very significant for SN-38 activity. The peak at 3550 cm^{-1} represents the hydroxyl vibration of the phenolic group of SN-38 in mNPs containing SN-38.

Differential scanning calorimetry (DSC)

The differential scanning calorimetry was conducted to investigate the thermal properties and the physical state of the drug in mNPs. The amorphous or crystalline properties of the drug can affect the in vitro and in vivo release. Chitosan exhibited an endothermic peak at 140 °C in Fig. 3, and HA showed a broad peak at 106 °C along with an exothermic peak at 239 °C. SN-38 showed an endothermic melting point at 287 °C and a characteristic peak at 225 °C, both of these two peaks have disappeared in the thermogram of mNPs Fig. 3**(D)**, this result could be that the SN-38 transformed into an amorphous state in mNPs. The amorphous state of SN-38 had better wettability and exhibited significant pharmacokinetic properties [31]. Finally, the disappearance of HA peaks indicated the interaction between HA, chitosan, and SN-38.

J. Mex. Chem. Soc. **2021**, *65*(4)
Regular Issue

ISSN-e 2594-0317

Adsorption isotherm study

Adsorption isotherm models including Langmuir, Freundlich, Temkin, and Sips were used to analyze the equilibrium isotherm data. The match between the models and equilibrium data was evaluated based on the determination coefficient (R^2).

Langmuir isotherm model

Langmuir isotherm assumes monolayer adsorption of adsorbate on the adsorbent surface and occurrence of homogenous adsorption, where each molecule adsorbs the same amount of constant energy and enthalpy [32] with no transmigration of the adsorbate [33]. The linear equation is presented in Equation (3):

$$\frac{C_e}{q_e} = \frac{C_e}{q_{max}} + \frac{1}{k_L q_{max}} \tag{3}$$

Where, q_e represents the adsorbed amount of SN-38 after reaching equilibrium (mg g^{-1}), C_e is the equilibrium concentration of SN-38 in the solution (mg L^{-1}), q_{max} denotes the maximum level of monolayer adsorption (mg g^{-1}), and k_L is Langmuir adsorption constant which is determined from the slope and the intercept of the linear plot respectively in Fig. 4**(A)**.

Freundlich isotherm model

The Freundlich isotherm assumes non-ideal and reversible adsorption on heterogeneous surfaces and multilayer physisorption [34,35]. The adsorption occurs on all sites of the adsorbent surface. The isotherm is described in Equation (4):

$$\log q_e = \log K_F + (\frac{1}{n}) \log C_e \tag{4}$$

Where, K_F ((mg g^{-1}) ((mg g^{-1}) $^{n-1}$)$^{-1)}$ and n could be determined from the intercept and slope of linear graph, which can be regarded as the capacity and strength of adsorption respectively, as shown in Fig. 4**(B)**. The slope ranges indicate the adsorption intensity or heterogeneity of the surface, with the value of n^{-1} determining the type of isotherm. If n^{-1} =0, it reveals the isotherm is irreversible and the surface is more heterogeneous, while 0 < n^{-1} < 1 suggests the isotherm is favorable and shows the adsorption intensity or surface heterogeneity. Finally, n^{-1} >1 shows an unfavorable isotherm or cooperative process [36,37].

Temkin isotherm model

Temkin model indicates adsorbent-adsorbate interactions and the extent of adsorption heat on the adsorbent surface. The coverage of adsorbent causes the heat of adsorption to decline linearly with this model (Equation (5)) showing that the distribution of binding energy is uniform.

$$q_e = B \ln A + B \ln C_e \tag{5}$$

Where, B is the Temkin constant related to the heat of sorption (kJ mol^{-1}) and A is the Temkin equilibrium binding constant (L mg^{-1}) corresponding to the maximum binding energy [38]. The parameters were obtained based on linear plots of q_e versus in C_e in Fig. 4**(C)**.

Sips isotherm model

The Sips isotherm model is a combination of Langmuir and Freundlich isotherm for predicting heterogeneous adsorption to overcome the drawbacks related to increased adsorption upon concentration rise [36,39]. The Sips equation is expressed as follows:

J. Mex. Chem. Soc. **2021**, *65*(4)
Regular Issue

ISSN-e 2594-0317

$$q_e = \frac{q_m k_s C_e^{ms}}{1+k_s C_e^{ms}} \quad (6)$$

where, C_e represents the equilibrium concentration (mg L^{-1}), q_m and K_s are the Sips maximum adsorption capacity (mg g^{-1}) and Sips equilibrium constant (L mg^{-1}), respectively, and *ms* is the Sips exponent. K_s and *ms* calculated from the slope and intercept of plot in Fig. 4**(D)**.

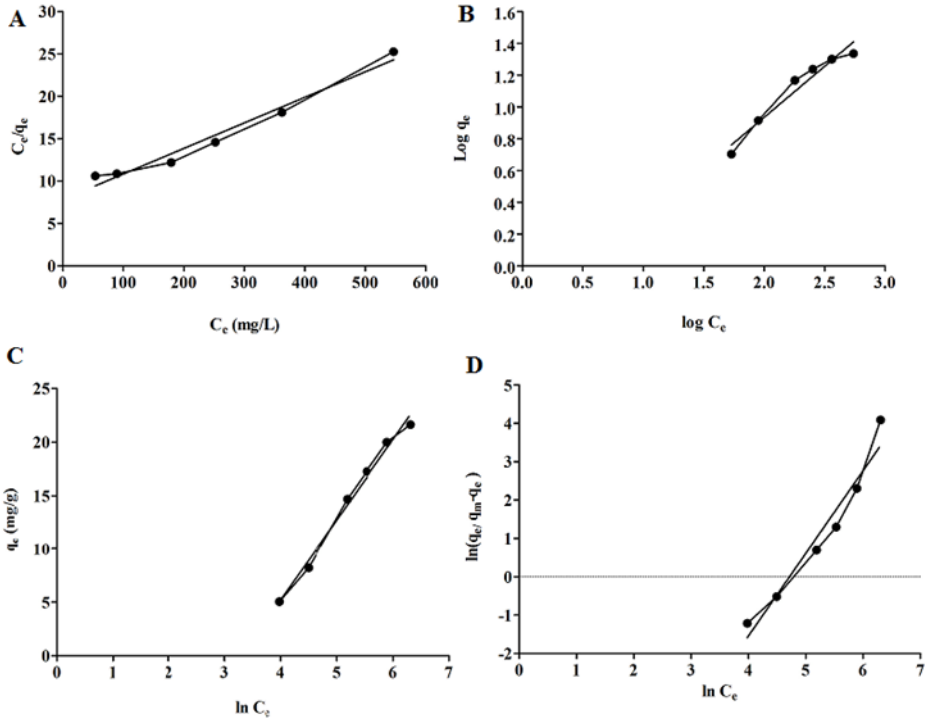

Fig. 4. Equilibrium adsorption isotherm, **(A)** Langmuir, **(B)** Freundlich, **(C)** Temkin, **(D)** Sips isotherms.

Fig. 4**(A-D)** and the data in Table 1 present all isotherm parameters. By comparing all the isotherm parameters, and the determination of the coefficient values, it can be found that the Langmuir equation has had the highest R^2 (0.9953) for the adsorption data over Temkin, Freundlich, and Sips (R^2 0.9898 > 0.9495> 0.9488). This result indicated the homogenous distribution of active sites on the surface of mNPs, after reaching equilibrium, the adsorption process continued in a monolayer pattern. The maximum adsorption capacity (q_m) of mNPs was obtained 346.511 mg g^{-1}. The magnitude of n constant in the Freundlich equation determines the type of adsorption, where n values >1 show favorable adsorption, meaning that a single layer of SN-38 molecules was formed on the surface of mNPs. In this study, n=1.5 signals favorable SN-38 adsorption. The low Temkin constant A (0.036 L mg^{-1}) revealed a weak interaction between SN-38 and mNPs suggesting the occurrence of physical adsorption [38]. Compared with previous literature, Dramou *et al.* [19] reported that conjugation of folic acid to chitosan –magnetic halloysite could yield the maximum adsorption capacity of 227.10 mg g^{-1} for adsorption of camptothecin (SN-38 group). Also, Itatahine *et al.* [19, 20] managed to improve the adsorption capacity of camptothecin to 200 mg g^{-1} using magnetic nanomaterials with these nanomaterials following the Langmuir isotherm adsorption. Hidaka et al. reported similar results in previous work for adsorption of SN-38 on oral adsorbent AST-120 (Kremezin) [40].

J. Mex. Chem. Soc. **2021**, *65*(4)
Regular Issue

ISSN-e 2594-0317

Table 1. Parameters of isotherm models regarding adsorption of SN-38 on mNPs.

Model	Isotherm constant	
Langmuir	q_m /mg g^{-1}	346.511
	K /L mg^{-1}	0.000315
	R^2	0.9953
Freundlich	K_F /((mg g^{-1}) ((mg g^{-1}) $^{n-1}$)$^{-1}$)	0.4470
	1/n	0.6423
	R^2	0.9495
Temkin	A / L mg^{-1}	0.036
	B /kj mol^{-1}	7.5415
	R^2	0.9898
Sips	K_s /L mg^{-1}	3.89E-05
	q_m /mg g^{-1}	30.27
	R^2	0.9488

Kinetic studies

To investigate the rate of SN-38 transport from the bulk dispersion to the surface of mNPs, two models: pseudo-first order and pseudo-second order were evaluated which determine the possible interaction between the adsorbent and adsorbate.

Pseudo-first order model

The pseudo-first-order kinetic adsorption model confirms that the number of adsorption sites depends on the free number of physisorption. The pseudo-first-order kinetic model is described by the following equation:

$$\frac{dq}{q_e - q} = k_1 dt \tag{7}$$

We have the following equation by integrating the equation for boundary conditions t=0 to t=t and q=0 to q=q_t,

$$ln(q_e - q_t) = ln\, q_e - k_1 t \tag{8}$$

q_e and q_t (mg g^{-1}) represent the amount of SN-38 adsorbed at equilibrium state and at interval time t respectively; K_1 (min^{-1}) is a pseudo-first order constant; t (min) denotes the time of adsorption process [19].

Pseudo-second order model

The pseudo-second order model confirms the chemical reaction between adsorbent and adsorbate, where the primary adsorption rate control occurs because of covalent/ionic interaction between the adsorbate and adsorbent. The linearized equation form is as the following equation:

$$\frac{1}{q_t} = \frac{1}{k_2 q_e^2 t} + \frac{1}{q_e} \tag{9}$$

Where, K_2 (g mg^{-1} min^{-1}) is a pseudo-second order constant.

The validity of adsorption kinetic models was determined by linear regression of adsorption kinetics, as shown in Fig. 5. The corresponding determination coefficients and kinetic parameters are reported in Table 2. The determination coefficient of pseudo-first-order kinetic ($0.97< R^2 <0.99$) was larger than that of pseudo–second-order kinetic ($0.91<R^2<0.99$). Further, in spite of the higher determination coefficient for pseudo-first-order, the values of $q_{e,\ experimental}$ obtained from Equation (8) were closer to $q_{e,\ calculated}$ values.

J. Mex. Chem. Soc. **2021**, *65*(4)
Regular Issue

ISSN-e 2594-0317

The results indicated that the nature of SN-38 adsorption process onto mNPs was physical adsorption, this physical adsorption of SN-38 due to the non-covalent adsorption like as cation- Π interaction between sodium of hyaluronic acid and SN-38, polar- Π interaction between OH groups of hyaluronic acid with aromatic rings of SN-38, the hydrogen bond interaction between of oxygen in the carbonyl group of SN-38 and OH group of hyaluronic acid were selected to load SN-38 on mPEG-chitosan/HA nanoparticles because of avoiding the use of chemical reaction and toxic junction reagents, which will not affect the activities of SN-38[41, 42] . Most of the previous literature indicated that the adsorption of SN-38 (camptothecin) and most anticancer drugs followed pseudo-second -order kinetic models, describing a chemisorption behavior [19, 29, 43]. Thus, in this study, no chemisorption between adsorbent and adsorbate would interfere with the complete release of hydrophobic SN-38 in the release media.

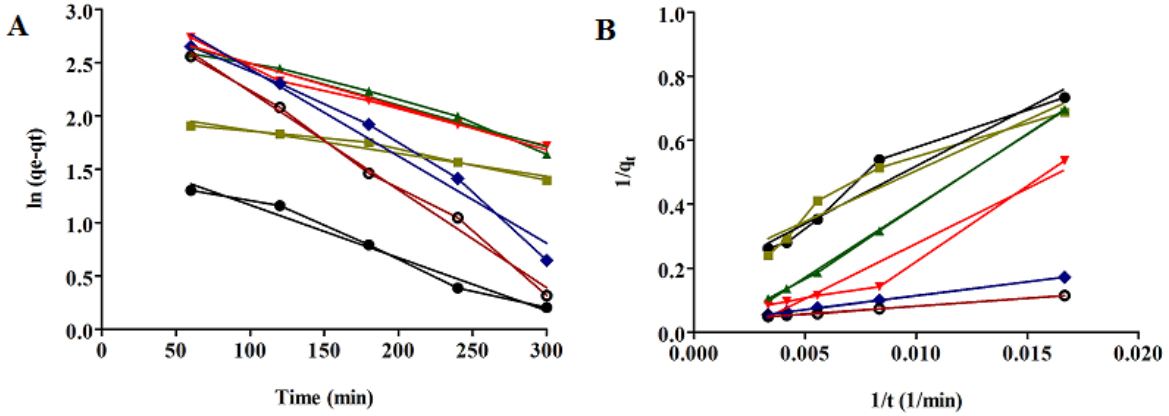

Fig. 5. Adsorption kinetics of SN-38 on mNPs, **(A)** pseudo-first-order **(B)** pseudo-second-order, 55 (mg L^{-1}) ●, 92 (mg L^{-1}) ■, 185 (mg L^{-1}) ◆, 260 (mg L^{-1}) ▲, 370 ◆, 555 (mg L^{-1}) ○.

Table 2. Parameters of adsorption kinetic models of SN-38 on mNPs.

C0/ mg L^{-1}	Pseudo-first-order				Pseudo-second-order		
	$q_{e.exp}$	$q_{e.cal}$	K_1	R^2	$q_{e.cal}$	K_2	R^2
55	5.04	5.10	0.0049	0.976	6.31	0.00065	0.9485
92	8.20	7.99	0.0021	0.961	5.34	0.0011	0.9193
85	14.69	14.15	0.0038	0.972	19.12	6.112E-05	0.9992
260	17.27	17.28	0.0040	0.974	14.92	0.0001	0.9406
370	20	19.68	0.0081	0.971	38.46	7.752E-05	0.9991
55	21.63	22.19	0.0091	0.993	31.25	0.0002	0.9985

Thermodynamic study

The thermodynamic parameters confirm whether the adsorption occurs spontaneously or not and offer information about the effect of temperature on the adsorption process. The Gibbs free energy can be calculated with changes in the temperature. For adsorption reactions, K_C is evaluated as follows:

$$K_C = \frac{C_s}{C_e} \tag{10}$$

where, C_s is the equilibrium concentration of SN-38 on NPs adsorbent and C_e denotes the equilibrium concentration of SN-38 in the dispersed solution. The changes in the free adsorption free energy (ΔG), enthalpy (ΔH), and entropy (ΔS) were calculated according to the following equations: [44]

J. Mex. Chem. Soc. **2021**, *65*(4)
Regular Issue

ISSN-e 2594-0317

$$\Delta G = -RT\ ln\ K_c \tag{11}$$

where, R is the universal gas constant (8.314J $K^{-1}.mol^{-1}$) and T is temperature in K. The average standard enthalpy change (ΔH) can be evaluated from Van't Hoff equation (12): [45]

$$ln\ K_C = \frac{-\Delta H}{RT} + \frac{\Delta S}{R} \tag{12}$$

The slope and intercept of equation (12) represent ΔH and ΔS respectively. The plot of ln K_c vs. T^{-1} for adsorption of SN-38 on mNPs is depicted in Fig. 6. Also, the thermodynamic parameters are presented in Table 3. In this table, the values of ΔG are between 0 and 20, indicating the adsorption process is physisorption [46]. Also, the negative ΔG values reveal that the adsorption process of SN-38 on mNPs is spontaneous. Moreover, the positive values of ΔH in Table 3 signal endothermic adsorption. Further, the values of ΔH lower than 40 kJ mol^{-1} confirm that the loading of SN-38 on mNPs is physical adsorption, and positive ΔS changes indicate randomness at the adsorbent-solution interface [47]. However, the magnitude of ΔS indicates no change in the structure of mNPs adsorbent during the adsorption process [38].

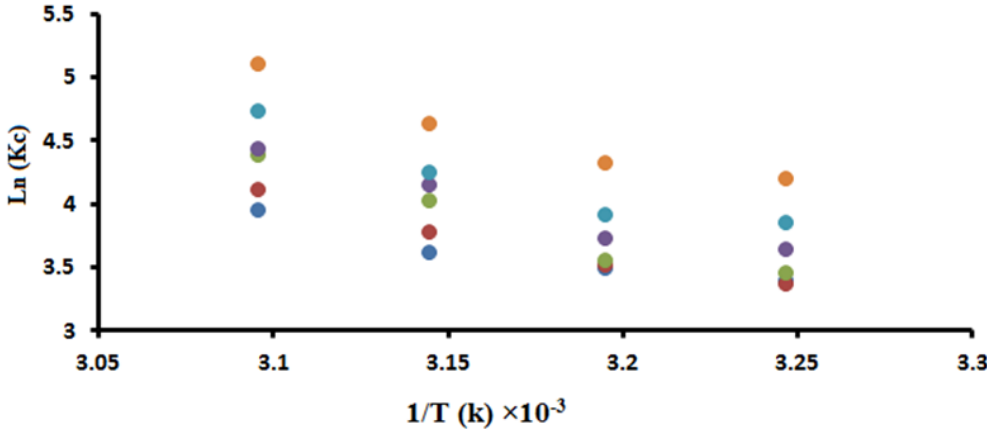

Fig. 6. The plot of ln K_c vs. 1/T ×10^3 for evaluating enthalpy and entropy change, 55●, 92 ●, 185●, 260●, 370●, 555 ●.

Table 3. Thermodynamic parameters of SN-38 adsorption on mNPs at different temperatures.

Concentration (mg l^{-1})	Temperature (K)	ΔG (kJ mol^{-1})	ΔH (kJ mol^{-1})	ΔS (J mol^{-1})
55	308	-8.660	25.402	111.47
	313	-9.063		
	318	-9.558		
	323	-10.591		
92	308	-8.625	25.415	111.98
	313	-9.129		
	318	-9.959		
	323	-11.040		
185	308	-8.845	26.870	118.85
	313	-9.230		
	318	-10.62		
	323	-11.768		
260	308	-9.307	26.871	118.97

J. Mex. Chem. Soc. **2021**, *65*(4)
Regular Issue

ISSN-e 2594-0317

	313	-9.669		
	318	-10.948		
	323	-11.890		
370	308	-9.861	26.970	120.34
	313	-9.669		
	318	-10.948		
	323	-11.890		
555	308	-10.724	29.132	130.65
	313	-11.218		
	318	-12.246		
	323	-13.704		

Ex- vivo release of SN-38 from mNPs

In this study, we used the rat intestine for measuring the transport of mNPs containing SN-38 and free SN-38 across the intestinal barrier [30]. As shown in Fig. 7, the transport of mNPs containing SN-38 from the intestinal barrier (17.4 %) was significantly ($p<0.01$) higher than that of free SN-38 (5.3 %). This improvement of transportation from the intestinal barrier could be related to the PEGylation of chitosan [16]. Therefore, PEGylated chitosan can improve the transport of SN-38 from the intestine, opens the tight junction [30, 48] and, can provide stealth properties to nanoparticles surface which cause the nanoparticles cannot be recognized by the immune system [49]. These results are in good accordance with previously published data [30]. Several mathematical equations were applied to study the kinetics of *ex-vivo* SN-38 dissolution. The mathematical models play a significant role to understand the drug release kinetics [50].

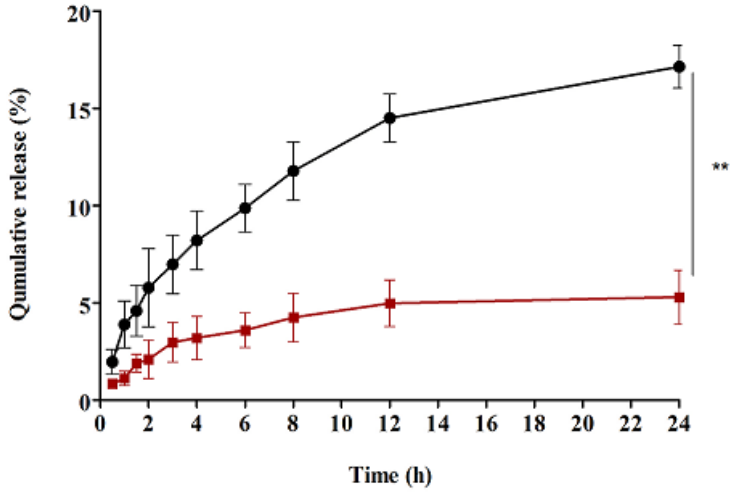

Fig. 7. The release profile of SN-38 from mNPs and free SN-38 in the medium (pH 7.4) as a function of time: mNPs containing SN-38 (●), free SN-38(■). The indicated values are means of at least three experiments ± SD (**p ≤ 0.01).

Zero-order model

The zero-order equation describes a system where the drug release rate is independent of its concentration and refers to constant drug release from a drug delivery agent. Thus, frequent repetitive dosing is required to maintain effective drug concentration, as such compliance and control are more difficult for patients [51]. The Zero-order release equation can be represented as follows:

J. Mex. Chem. Soc. **2021**, *65*(4)
Regular Issue

ISSN-e 2594-0317

$$C = C_0 + K_0 t \quad (13)$$

Where, C is the extent of drug release, C_0 is the initial amount of the drug in solution, and K_0 is the zero-order release constant. The release profile of SN-38 is presented in Table 4. The result shows that SN-38 release from mNPs (R^2=0.8507) and free SN-38 (R^2=0.8959) does not follow the zero-order kinetics.

Table 4. Results of Different models in terms of R^2, slope and intercept.

Model name	Release of SN-38 from mNPs			Release of free SN-38		
	R^2	slop	Intercept	R^2	Slop	intercept
Zero order	0.8507	0.6210	0.09197	0.8959	0.1819	0.03952
First order	0.6225	0.03131	0.008621	0.5400	0.02737	0.00893
Higuchi	0.9717	3.767	0.1885	0.8992	1.195	0.1174
Hixon-Crowell	0.7122	0.0481	1.667	0.60666	0.02927	1.221

First-order equation

The first-order equation depends on the concentration gradients between the static liquid layer next to mNPs and bulk liquid. This equation considers no change in the shape of solid during dissolution.

$$log\, C = log\, C_0 - k_1 t/2.303 \quad (14)$$

Where, K_1 (h^{-1}) is the first-order rate equation expressed by time. The slope of dissolution of the drug in the *Ex-vivo* plot vs. time gives the first-order kinetic constant. The result in Table 4 shows that the cumulative release against time does not follow the first order. The determination coefficient of mNPs containing SN-38 (R^2=0.6225) and free SN-38 (R^2=0.5425) is low.

Higuchi model

Higuchi tries to explain the release of the drug from the drug delivery system which involves dissolution and diffusion. It involves penetration of the surrounded liquid to dissolve the drug and draining out through pores and channels [52].

$$Q = k_H t^{0.5} \quad (15)$$

Where, K_H ($h^{-1/2}$) is the Higuchi dissolution constant. As shown in Table 4, the determination coefficient of mNPs containing SN-38 (R^2=0.9717) well matches the data of dissolution.

Hixson-Crowell

Hixson equation describes the changes in the surface area and particle diameter. The equation is as follows:

$$Q_0^{1/3} - Q_t^{1/3} = k_{HC} t \quad (16)$$

Where, Q_0 is the initial amount of the SN-38, Q_t denotes the amount of the drug release at time t, and K_{HC} ($h^{-1/3}$) is Hixon-Crowell constant. This equation predicts that the surface area of mNPs changes with dissolution. The determination coefficients of this equation for mNPs containing SN-38 (R^2=0.7122) and for free SN-38 (R^2=0.6066) are very low (Table 4). Therefore, this equation cannot evaluate the solubility.

Korsmeyer-Peppas Model

Korsmeyer described drug release from a polymeric system as follows.

J. Mex. Chem. Soc. **2021**, *65*(4)
Regular Issue

ISSN-e 2594-0317

$$\frac{M_t}{M_\infty} = kt^n \quad (17)$$

Where, $M_t/M\infty$ defines the release of drug at time t. The values of n are used to determine the different release mechanism, n=0.45 for Fickian diffusion, 0.45<n<0.89 for non-Fickian transport, n=0.89 case –Π transport, and n>0.89 super case–Π transport [53].

As presented in Fig.8, mNPs containing SN-38 show a good concordance between dissolution data and Korsmeyer-peppas kinetic model (R^2=0.9826). The drug release mechanism is obtained from the exponent of the release mechanism. n=0.5953 shows non-Fickian or anomalous transport, where the drug release mechanism could be governed by diffusion and swelling [54]. Non-Fickian dissolution occurs in vitreous polymers, where the polymer chains rearrange slowly, and the diffusion occurs with the same ratio [55]. The diffusion and swelling rates are relative, where the polymer relaxation and solvent diffusion have a similar significance [56]. According to the analysis of the above results, the release of free SN-38 follows the Higuchi model (R^2=0.8992) and that of mNPs containing SN-38 follows Korsmeyer-peppas model (R^2=0.9826). Therefore, these two release models are sustained release mechanisms, but in the Higuchi model, it is assumed that the matrix contains an initial drug concentration far higher than the solubility of the drug, which indicates that this model is constrained by the drug delivery system [52]. Incorporating SN-38 into mNPs not only improved the drug release, but also modified the release mathematical model [30].

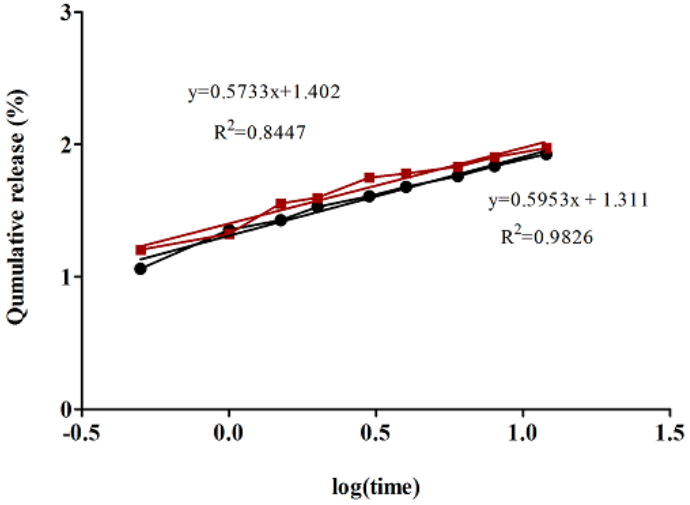

Fig. 8. Korsmeyer-peppas kinetic model of SN-38 from mNPs and free SN-38 in medium (pH 7.4) as a function of time: mNPs containing SN-38 (●), free SN-38 (■).

A comparison of mNPs as an efficient adsorbent with the literature data

Table 5 compares mNPs and the other adsorbents for adsorption of SN-38 [57-66].

Nevertheless, the experimental conditions to obtain the adsorbents were different and the direct comparison was not feasible. The q_{max} values were different for various adsorbents, but the maximum adsorption capacity of mNPs is 346.511 mg/g, suggesting that mNPs are a good candidate for physical adsorption of SN-38 for drug delivery. The hydrogen bonding between polymers and two hydroxyl groups of SN-38 caused greater adsorption of the anticancer drug on nanocarriers such as mNPs [3]. It can be concluded that, the combination of three biodegradable polymers (mPEG, chitosan and HA) could be proved a promising carrier for drug delivery and biological applications [28].

J. Mex. Chem. Soc. **2021**, *65*(4)
Regular Issue

ISSN-e 2594-0317

Table 5. Comparing of mNPs adsorbent with other different literature adsorbents.

Adsorbent	Capacity adsorbent/ mg g^{-1}	References
magnetic nanoparticles modified by (3-aminopropyl) triethoxysilane	85	[57]
poly(anhydride) nanoparticles and cyclodextrins	50	[57]
methoxy poly(ethylene glycol)-b-poly(ε-caprolactone)	96	[59]
poly(ethylene glycol)-dihydrolipoic acid (MeO-PEG2k-DHLA)	318	[60]
zeolitic imid-azolate framework-8	10	[61]
mPEG-PCL and mPEG-PLGA	33.7	[62]
polyelectrolyte complex nanoparticles	111	[63]
α-CD-GO-Fe3O4	210	[64]
γ-CD-GO-Fe3O4	220	
poly(ethylene glycol)-block-poly(propylene glycol)-block-poly(ethylene glycol) (Pluronic F-108)	207	[65]
graphene oxides –polyvinylpyrrolidone (GO-PVP)	170	[66]
graphene oxides –β –cyclodextrin (GO-β-CD)	140	
mPEG-Chitosan/HA	346.511	This work

Conclusion

In this study, a biocompatible biopolymer with a low-toxic safe method was used to synthesize a new adsorbent. This novel adsorbent was synthesized by conjugating of poly- (ethylene glycol)-methyl ether (mPEG) to chitosan followed ionic gelation between mPEG-chitosan and hyaluronic acid (HA) to produce mNPs adsorbent particles. The adsorbent was characterized by FT-IR, DSC and SEM. The prepared mNPs were used to adsorption/release of 7-ethyl-10-hydroxycamtothecin (SN-38) anticancer from its liquid dispersions. Further, the isotherm models revealed that adsorption of SN-38 on mPNs follows the Langmuir model and suggested the monolayer sorption. Also, the kinetic and thermodynamic (ΔH, ΔG and ΔS) studies confirm the physical adsorption of SN-38 on the mNPs is predominant. Moreover, the release of SN-38 from mNPs indicated that the release of SN-38 from mNPs governed by diffusion process. The results showed the prepared mNPs as compared to other SN-38 delivery systems appear to be safe and are a promising way for oral delivery.

Acknowledgements

The financial support was provided by the Research Vice Presidency of Semnan University and Mazandaran University of Medical Science.

References

1. Fang, J.-Y.; Hung, C.-F.; Hua, S.-C.; Hwang, T.-L. *Ultrasonics.* **2009,** *49*, 39-46
2. Ebrahimnejad, P.; Dinarvand, R.; Sajadi, A., *J. Food Drug Anal.* **2009**, *17*.
3. Einafshar, E.; Asl, A. H.; Nia, A. H.; Mohammadi, M.; Malekzadeh, A.; Ramezani, M. *Carbohydr. Polym.* **2018**, *194*, 103-110.

J. Mex. Chem. Soc. **2021**, *65*(4)
Regular Issue

ISSN-e 2594-0317

4. Sahoo, N. G.; Bao, H.; Pan, Y.; Pal, M.; Kakran, M.; Cheng, H. K. F.; Li, L.; Tan, L. P. *Chem. Commun.* **2011**, *47*, 5235-5237.
5. Mohammady, H.; Dinarvand, R.; Esfandyari Manesh, M.; Ebrahimnejad, P. *Nanomed. J.* **2016**, *3*, 159-168.
6. Yang, Z.; Luo, H.; Cao, Z.; Chen, Y.; Gao, J.; Li, Y.; Jiang, Q.; Xu, R.; Liu, J., *Nanoscale.* **2016**, *8*, 11543-11558.
7. England, R. M.; Hare, J. I.; Barnes, J.; Wilson, J.; Smith, A.; Strittmatter, N.; Kemmitt, P. D.; Waring, M. J.; Barry, S. T.; Alexander, C. *J. Controlled Release.* **2017**, *247*, 73-85.
8. Lee, S.-Y.; Yang, C.-Y.; Peng, C.-L.; Wei, M.-F.; Chen, K.-C.; Yao, C.-J.; Shieh, M.-J. *Biomaterials.* **2016**, *86*, 92-105.
9. Butler, K. S.; Durfee, P. N.; Theron, C.; Ashley, C. E.; Carnes, E. C.; Brinker, C. J. *Small.* **2016**, *12*, 2173-2185.
10. Sharifi, F.; Nazir, I.; Asim, M. H.; Jahangiri, M.; Ebrahimnejad, P.; Matuszczak, B.; Bernkop-Schnürch, A. *J. Mol. Liq.* **2019**, *291*, 111285.
11. Toole, B. P. *Nat. Rev. Cancer.* **2004**, *4*, 528-539.
12. Sadeghi Ghadi, Z.; Ebrahimnejad, P. *J. Microencapsulation.* **2019**, *36*, 169-179.
13. Dang, J. M.; Leong, K. W. *Adv. Drug Delivery Rev.* **2006**, *58*, 487-499.
14. Al-Qadi, S.; Alatorre-Meda, M.; Zaghloul, E. M.; Taboada, P.; Remunán-López, C., *Colloids Surf.* **2013,** *103*, 615-623.
15. Mir, M.; Ebrahimnejad, P. *Nanoscience & Nanotechnology-Asia.* **2014**, *4*, 80-87.
16. Dong, Y.; Feng, S.-S. *Biomaterials.* **2004**, *25*, 2843-2849.
17. Venkataraman, S.; Hedrick, J.; Ong, Z. *Adv. Drug Delivery Rev.* **2011**, *63*, 1228.
18. O'neill, V.; Twelves, C. *Br. J. Cancer.* **2002**, *87*, 933-937.
19. Dramou, P.; Fizir, M.; Taleb, A.; Itatahine, A.; Dahiru, N. S.; Mehdi, Y. A.; Wei, L.; Zhang, J.; He, H. *Carbohydr. Polym.* **2018**, *197*, 117-127.
20. Itatahine, A.; Mehdi, Y. A.; Fizir, M.; Qi, M.; Dramou, P.; He, H. *New J. Chem.* **2018**, *42*, 1326-1336.
21. Kar, K. K. *Carbon nanotubes: synthesis, characterization and applications*. Research Publishing Service: 2011.
22. Matsumura, Y. *Adv. Drug Delivery Rev.* **2008**, *60*, 899-914.
23. Chen, K.-J.; Tang, L.; Garcia, M. A.; Wang, H.; Lu, H.; Lin, W.-Y.; Hou, S.; Yin, Q.; Shen, C. K.-F.; Cheng, J. *Biomaterials.* **2012**, *33*, 1162-1169.
24. Zhuang, J.; Kuo, C.-H.; Chou, L.-Y.; Liu, D.-Y.; Weerapana, E.; Tsung, C.-K. *ACS nano.* **2014**, *8*, 2812-2819.
25. Chi, Y.; Wang, Z.; Wang, J.; Dong, W.; Xin, P.; Bi, J.; Jiang, T.; Chen, C.-P. *Colloid Polym. Sci.* **2020**, *298*, 51-58.
26. Su, X.; Wu, L.; Hu, M.; Dong, W.; Xu, M.; Zhang, P. *Biomed. Pharmacother.* **2017**, *95*, 670-678.
27. Kulkarni, A. R.; Hukkeri, V. I.; Sung, H. W.; Liang, H. F. *Macromol. Biosci.* **2005**, *5*, 925-928.
28. Yang, L.; Gao, S.; Asghar, S.; Liu, G.; Song, J.; Wang, X.; Ping, Q.; Zhang, C.; Xiao, Y. *Int. J. Biol. Macromol.* **2015**, *72*, 1391-1401.
29. Wu, S.; Zhao, X.; Li, Y.; Du, Q.; Sun, J.; Wang, Y.; Wang, X.; Xia, Y.; Wang, Z.; Xia, L. *Materials.* **2013**, *6*, 2026-2042.
30. Saremi, S.; Atyabi, F.; Akhlaghi, S. P.; Ostad, S. N.; Dinarvand, R. *Int. J. Nanomed.* **2011**, *6*, 119.
31. Sun, X.; Zhu, D.; Cai, Y.; Shi, G.; Gao, M.; Zheng, M. *Int. J. Nanomed.* **2019**, *14*, 2115.
32. Dada, A.; Olalekan, A.; Olatunya, A.; Dada, O. *IOSR J. Appl. Chem.* **2012**, *3*, 38-45.
33. Sharma, Y.; Srivastava, V.; Upadhyay, S.; Weng, C. *Ind. Eng. Chem. Res.* **2008**, *47*, 8095-8100.

J. Mex. Chem. Soc. **2021**, *65*(4)
Regular Issue

ISSN-e 2594-0317

34. Alimohammady, M.; Jahangiri, M.; Kiani, F.; Tahermansouri, H. *J. Environ. Chem. Eng.* **2017**, *5*, 3405-3417.
35. Davodi, B.; Jahangiri, M.; Ghorbani, M. *Part. Sci. Technol.* **2019**, 1-12.
36. Kumar, V. *Arabian J. Chem.* **2019**, *12*, 316-329.
37. Alimohammady, M.; Jahangiri, M.; Kiani, F.; Tahermansouri, H. *Res. Chem. Intermed.* **2018**, *44*, 69-92.
38. Khan, T. A.; Chaudhry, S. A.; Ali, I. *J. Mol. Liq.* **2015**, *202*, 165-175.
39. Anbia, M.; Mohammadi Nejati, F.; Jahangiri, M.; Eskandari, A.; Garshasbi, V. *J. Sci., Islamic Repub. Iran.* **2015**, *26*, 213-222.
40. Hidaka, M.; Yamasaki, K.; Okumura, M.; Ogikubo, T.; Iwakiri, T.; Setoguchi, N.; Nishida, K.; Nagai, K.; Ikenoue, T.; Arimori, K. *Cancer Chemother. Pharmacol.* **2007**, *59*, 321-328.
41. Guo, M.; Rong, W.-T.; Hou, J.; Wang, D.-F.; Lu, Y.; Wang, Y.; Yu, S.-Q.; Xu, Q. *Nanotechnology.* **2013**, *24*, 245101-245120.
42. Prasad, S.; Dangi, J. *Artif. Cells, Nanomed., Biotechnol.* **2016**, *44*, 1824-1834.
43. Malek, S. K.; Gabris, M. A.; Jume, B. H.; Baradaran, R.; Aziz, M.; Karim, K. J. B. A.; Nodeh, H. R. *Daru, J. Pharm. Sci.* **2019**, *27*, 9-20.
44. Akçay, G.; Kılınç, E.; Akçay, M. *Colloids Surf. A.* **2009**, *335*, 189-193.
45. Morton III, S. A.; Keffer, D. J.; Counce, R.; DePaoli, D.; Hu, M.-C. *J. Colloid Interface Sci.* **2004**, *270*, 229-241.
46. Gereli, G.; Seki, Y.; Kuşoğlu, İ. M.; Yurdakoç, K. *J. Colloid Interface Sci.* **2006**, *299*, 155-162.
47. Karaca, S.; Gürses, A.; Ejder, M.; Açıkyıldız, M. *J. Colloid Interface Sci.* **2004**, *277*, 257-263.
48. Choi, K. Y.; Min, K. H.; Yoon, H. Y.; Kim, K.; Park, J. H.; Kwon, I. C.; Choi, K.; Jeong, S. Y. *Biomaterials.* **2011**, *32*, 1880-1889.
49. Hussain, Z.; Khan, S.; Imran, M.; Sohail, M.; Shah, S. W. A.; de Matas, M. *Drug Delivery Transl. Res.* **2019**, *9*, 721-734.
50. Gouda, R.; Baishya, H.; Qing, Z. *J. Dev. Drugs.* **2017**, *6*.
51. Walters, K. A.; Brain, K. R. Dermatological formulation and transdermal systems. In *Dermatological and transdermal formulations*, CRC Press, **2002**, 337-418.
52. Omidian, H.; Park, K., Introduction to hydrogels. In *Biomedical applications of hydrogels handbook*, Springer, **2010**, 1-16.
53. Korsmeyer, R. W.; Gurny, R.; Doelker, E.; Buri, P.; Peppas, N. A. *Int. J. Pharm.* **1983**, *15*, 25-35.
54. Klech, C. M.; Simonelli, A. P. *J. Membr. Sci.* **1989**, *43*, 87-101.
55. Peppas, N. A.; Narasimhan, B. *J. Controlled Release.* **2014**, *190*, 75-81.
56. Kosmidis, K.; Argyrakis, P.; Macheras, P. *J. Chem. Phys.* **2003**, *119*, 6373-6377.
57. Yamaura, M.; Camilo, R.; Sampaio, L.; Macedo, M.; Nakamura, M.; Toma, H. *J. Magn. Magn. Mater.* **2004**, *279*, 210-217.
58. Agüeros, M.; Zabaleta, V.; Espuelas, S.; Campanero, M.; Irache, J. *J. Controlled Release.* **2010**, *145*, 2-8.
59. Yue, X.; Qiao, Y.; Qiao, N.; Guo, S.; Xing, J.; Deng, L.; Xu, J.; Dong, A. *Biomacromolecules.* **2010**, *11*, 2306-2312.
60. Ling, L.; Ismail, M.; Du, Y.; Xia, Q.; He, W.; Yao, C.; Li, X. *Mol. Pharmaceutics.* **2018**, *15*, 5479-5492.
61. Zhang, Z.; Xu, Y.; Zhao, K.; Zhang, Y.; Chen, W.; Li, X.; Meng, Y.; Yang, D.; Wang, P.; Zhu, J. *Med. Res.* **2020**, *3*.
62. Gan, M.; Zhang, W.; Wei, S.; Dang, H. *Artif. Cells, Nanomed., Biotechnol.* **2017**, *45*, 389-397.

J. Mex. Chem. Soc. **2021**, *65*(4)
Regular Issue

ISSN-e 2594-0317

63. Dinarvand, M.; Kiani, M.; Mirzazadeh, F.; Esmaeili, A.; Mirzaie, Z.; Soleimani, M.; Dinarvand, R.; Atyabi, F. *Int. J. Biol. Macromol.* **2015**, *78*, 112-121.
64. Patil, A.; Nimbalkar, M.; Patil, P.; Chougale, A.; Patil, P. *Mater. Today: Proc.* **2020**, *23*, 437-443.
65. Chen, D.; Bi, J.; Wu, J.; Kumar, A. *J. Inorg. Organomet. Polym. Mater.* **2020**, *30*, 573-579.
66. Karki, N.; Tiwari, H.; Pal, M.; Chaurasia, A.; Bal, R.; Joshi, P.; Sahoo, N. G. *Colloids Surf.* **2018**, *169*, 265-272.